*American Mineralogist, Volume 61, pages 1226–1240, 1976*

# Braunite: its structure and relationship to bixbyite, and some insights on the genealogy of fluorite derivative structures

PAUL B. MOORE AND TAKAHARU ARAKI

*Department of the Geophysical Sciences*
*The University of Chicago*
*Chicago, Illinois 60637*

**Abstract**

Braunite, $Mn^{2+}Mn_6^{3+}SiO_{12}$, $a$ = 9.408(16), $c$ = 18.668 (32)Å, tetragonal holosymmetric, space group $I4_1/acd$, $Z$ = 8, is a derivative structure of fluorite with ordered anion vacancies. $R$ = 0.036 ($Rw$ = 0.050) for 511 non-zero reflections.

The structures of cubic and orthorhombic bixbyite ($\alpha$–$Mn_2O_3$), braunite, and probably braunite-II ($Mn^{2+}Mn_{14}^{3+}SiO_{24}$), are related according to the space group *Ibca*. The regions in common include sheets of edge- and corner-linked octahedra (the *A* and *A'* sheets of bixbyite). Braunites differ in having *B* sheets in place of the *A'* sheets in bixbyite. The *B* sheets consist of $Mn^{2+}$ in cubic coordination, $Mn^{3+}$ in octahedral coordination, and $Si^{4+}$ in tetrahedral coordination with respect to oxygen.

Average polyhedral distances are $^{(8)}Mn(1)^{2+}$–O 2.33, $^{(6)}Mn(2)^{3+}$–O 2.04, $^{(6)}Mn(3)^{3+}$–O 2.05, $^{(6)}Mn(4)^{3+}$–O 2.04, and $^{(4)}Si$–O 1.61Å. The $Mn^{3+}O_6$ groups are distorted as a result of Jahn-Teller effects, forming elongate tetragonal bipyramids which are further distorted by shared polyhedral edges.

With help from an enumeration theorem, a cooperative lattice game is proposed which conveniently classifies all structures derived from fluorite.

## Introduction

Braunite has been a crystal-chemical enigma since it was first characterized by Haidinger in 1831. Variously interpreted as $(Mn,Si)_2O_3$, $3Mn^{2+}Mn^{4+}O_3 \cdot MnSiO_3$ or $3Mn_2O_3 \cdot MnSiO_3$, the problematical compound has been a center of controversy concerning the role of silica and the oxidation states of the transition metal. Dispute also centered around its crystal class and space group: Aminoff (1931) proposed the space group $I4_1/acd$ and Byström and Mason (1943) proposed $I\bar{4}c2$, the latter study including a crystal structure analysis. In addition, they concluded that the correct formula was $3Mn_2O_3 \cdot MnSiO_3$. Those authors also presented an account of earlier studies on the species.

There the matter stood until de Villiers and Herbstein (1967) investigated braunites from several localities and concluded from single crystal study that the space group was in fact $I4_1/acd$, the group originally proposed by Aminoff. A variant of braunite (braunite-II) was also characterized, which required a doubling of the $c$ axis, a halving of the amount of $SiO_2$, but a space group which was the same as ordinary braunite. The question then arose as regards the correct crystal structure, the relationship between the two braunites, and their relationship with bixbyite, $\alpha$–$Mn_2O_3$. With these facts at hand, we concluded that the braunite problem required further study.

We have also explored more deeply the subtle relation between braunite and bixbyite with the large family of anion-deficient fluorite derivative structures. Perhaps the most intriguing part of this study is not the braunite structure *per se*, but its relationship with other equally complex compounds.

## Experimental

A single crystal of braunite was selected from a specimen from St. Marcel, Piedmont, Italy, originally from the collection of George L. English (University of Chicago number 1663). Gorgeu (1893) reported MnO 74.40; O 7.50; $Fe_2O_3$, $Al_2O_3$ 3.80; CaO 0.50; MgO, $K_2O$, $Na_2O$ 1.00; PbO, CuO 0.15; CoO 0.30; BaO trace; $H_2O$ 0.20; $SiO_2$ 9.80; $P_2O_5$ 0.05, gangue 2.60 percent for Piedmont material. Accepting the sum of cations = 8 and the sum of $O^{2-}$ = 12, the

formula unit contains $(Mn^{2+}_{0.78}Mg^{3+}_{0.16}Ca^{3+}_{0.06})(Mn^{3+}_{5.71}Fe^{3+}_{0.29})Si^{4+}_{1.00}O_{12}$.

The crystal measured 0.140 mm along $a_1$, 0.137 mm along $a_2$ and 0.137 mm along $c$ and was mounted on a Pailred semi-automated diffractometer with an $a$ axis parallel to the machine rotation axis. Utilizing graphite-monochromatized Mo$K\alpha_1$ radiation ($\lambda$ = 0.70926Å), reflections with indices $hkl$, $hk\bar{l}$ ($h \geqq k$) were gathered to $k = 10$ with an upper limit of $\sin\theta/\lambda = 0.80$ on each level. Other details: scan speed 1° min$^{-1}$, 20 second stationary background measurements on each side of the peak, scan width range of 4.2°.

Absorption correction employed the Gaussian integration method (Burnham, 1966) with ten faces approximating the crystal shape. The maximum transmission factor computed to 0.414 and the minimum, 0.305. Unobserved reflections with intensity less than $2\sigma(I)$ were set $I_0 = \sigma(I)$. After the corrections for absorption, Lorentz, and polarization factors, equivalent reflection pairs $I(hkl)$ and $I(hk\bar{l})$ were averaged; 896 independent $|F_0|$ were available for the ensuing study.

The cell parameters for braunite were more precisely ascertained by a powder diffractometric trace on the same sample (Cu$K\alpha_1$ radiation, graphite monochromator, 1/2° min$^{-1}$ scan speed). The trace was corrected for absorption by the sample and alignment of the specimen slide. Twenty-nine indexed lines were used in a least-squares refinement, the results of which appear in Table 1.

### Solution and refinement of the structure

Since the space group we determined for braunite did not match that of Byström and Mason (1943), we assumed that the structure of our crystal was unknown. Further on, we will discuss the relationship between the two.

Three-dimensional Patterson synthesis, $P(uvw)$, indicated a structure based on fluorite, with $a' = a/2$ and $c' = c/4$ as the subcell period. This required that all cation positions be occupied but that vacancies occurred in the anion positions. Since we did not detect any violations of the space group $I4_1/acd$ (which is uniquely determined), severe restrictions were place on atom locations and the structure was solved without difficulty. The trial parameters for all independent cations were used toward a $\beta$ synthesis (Ramachandran and Srinivasan, 1970) from which the anion positions were recovered.

The trial structure consisted of one cation in cubic coordination, one in tetrahedral coordination, and three independent cations in octahedral coordination. Approximate bond distances revealed that $Si^{4+}$ alone appeared in the tetrahedral site. From the unit formula we assigned $Mn(1) = 0.78Mn^{2+} + 0.16Mg^{2+} + 0.06Ca^{2+}$ to the cubic site, and the trivalent ($Mn^{3+} + Fe^{3+}$) cations were distributed equally over the octahedral sites. This leads to 19.3 electrons at the Mn(1) site instead of 23 for $Mn^{2+}$, yielding an "occupancy" of 0.84 if the $Mn^{2+}$ scattering curve is used.

For refinement, we employed $Mn^{2+}$ for Mn(1), Mn(2), Mn(3), and Mn(4), $Si^{4+}$ for Si, and $O^{1-}$ for oxygen. X-ray scattering factors were obtained from the tables of Cromer and Mann (1968). Anomalous dispersion correction employed the tables of Cromer and Liberman (1970). Full-matrix least-squares refinement proceeded from FLMXLS, a program developed by T. Araki with options for bond distances and angles, derived from the familiar ORFLS program of Busing *et al.* (1962). The final cycle included one scale factor, one secondary extinction coefficient (Zachariasen, 1968), eight atomic coordinate parameters, thirty-seven anisotropic thermal vibration parameters and one occupancy parameter for Mn(1). At convergence, $R = 0.076$ and $R_w = 0.072$ for all 896

TABLE 1. Braunite and related compounds. Structure cell parameters

| | Braunite | | Braunite-II | Bixbyite | |
|---|---|---|---|---|---|
| a(Å) | 9.408(16) | 9.41(1) | 9.440(5) | 9.4146(1) | 9.4157(3) |
| b(Å) | - | - | - | - | 9.4233(3) |
| c(Å) | 18.668(32) | 18.64(2) | 37.76(1) | - | 9.4047(3) |
| Space group | $I4_1/acd$ | $I\bar{4}c2$ | $I4_1/acd$ | Ia3 | Pcab |
| Z | 8 | | 8 | 16 | 16 |
| Formula | $(Mn,Ca)^{2+}Mn^{3+}_8SiO_{12}$ | | $(Ca,Mn)^{2+}Mn^{3+}_{14}SiO_{24}$ | $(Mn_{0.98}Fe_{0.02})_2O_3$ | $Mn_2O_3$ |
| Reference | This study | Byström and Mason (1943) | de Villiers and Herbstein (1967) | Geller (1971) | |

TABLE 2. Braunite. Atom coordinates*

| | | | x | y | z |
|---|---|---|---|---|---|
| Mn(1) | 8 | 222 | 0 | 1/4 | 1/8 |
| Mn(2) | 16 | $\bar{1}$ | 0 | 0 | 0 |
| Mn(3) | 16 | 2 | 1/4 | 0.2157(1) | 0 |
| Mn(4) | 16 | 2 | 0.2318(1) | 1/4 + x | 1/8 |
| Si | 8 | $\bar{4}$ | 0 | 1/4 | 3/8 |
| O(1) | 32 | 1 | 0.1487(4) | 0.8537(4) | 0.9453(2) |
| O(2) | 32 | 1 | 0.1457(3) | 0.0734(3) | 0.0569(2) |
| O(3) | 32 | 1 | 0.0787(4) | 0.1347(3) | 0.9250(2) |

*Estimated standard errors in parentheses refer to the last digit. The atoms designated are followed by the number of positions and point symmetry.

reflections; and $R = 0.036$ and $R_w = 0.050$ for the 511 reflections above background error where $R_w = [\sum_w(|F_o| - |F_c|)^2/\sum_w F_o^2]^{1/2}$, with $w = \sigma_{F_o}^{-2}$. The "goodness of fit," $S = \sum_w||F_o| - |F_c||^2/(n-m)$, where $n$ = number of independent $F$'s and $m$ = number of parameters, is 1.23. The secondary extinction coefficient, $c_0$, is $2.0(3) \times 10^{-7}$ and the scale factor, $s$, is 0.810(5). Finally, the "occupancy" parameter for Mn(1) is 0.828(6), in good agreement with the chemical analysis for St. Marcel braunite. Thus, the minor $Ca^{2+}$ and $Mg^{2+}$ substitute at this site.

Table 2 lists the atomic coordinates, Table 3 the anisotropic thermal vibration parameters, and Table 4 the root-mean-square displacements and the orientations of the ellipsoids of vibration. Table 5 lists the structure factors[1] and Table 6 the polyhedral interatomic distances and angles.

### Braunite and bixbyite: group subgroup relationships

The structures of bixbyite and braunite are related, but they are not isomorphic. We inquire as to what extent they are related, and proceed by examining group–subgroup relationships between the two and seek out those subsets of the equivalent point sets which are isomorphic in the two structures.

Bixbyite and braunite are metrically related (Table 1) and differ by the $c$-crystallographic axis of braunite being double that of bixbyite. Geller (1971), in a detailed analysis of structures of synthetic bixbyites, noted that pure $\alpha$-$Mn_2O_3$ crystallizes in space group *Pcab* but that small amounts of $Fe^{3+}$ result in bixbyites with space group *Ia*3. Metrically, both kinds of bixbyite possess approximately the same cell parameters and differ only in distortion from cubic symmetry for the orthorhombic crystal. To the 48 equivalent oxygen atoms in a cell of cubic bixbyite there correspond 6 sets of 8 equivalent oxygen atoms in the orthorhombic bixbyite. Two questions then arise regarding bixbyite and braunite: do similar group-subgroup relations exist between the two, and to what extent is the isomorphism of the oxygen packing conserved?

It is convenient to inquire first about their space groups. Braunite crystallizes in space group $I4_1/acd$ and cubic bixbyite in *Ia*3. But $I4_1/acd$ is not a subgroup of *Ia*3, since the elements of the former are not contained in the latter when either one or two unit cells of *Ia*3 are considered. Rather, the nearest subgroup relation is $Ia3d(a_1,a_2,a_3) \rightarrow I4_1/acd(a_1,a_2,c = a_3)$. We then ask what is the maximal subgroup common to $I4_1/acd(a_1,a_2,c = 2a_3)$ and $Ia3(a_1,a_2,a_3)$. This is *Ibca* and its multiplication table is given in Table 7. The formal relation is $S(I4_1/acd{:}a_1,a_2,c) \cap S(Ia3{:}a_1,a_2,a_3) = S(Ibca{:}a,b,c)$, where the $S$ is the set of symmetry elements and $\cap$ denotes intersection. The group–subgroup relationship can be shown diagrammatically, *viz.*:

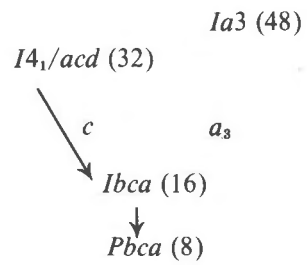


This states that for the equivalent points in $I4_1/acd$ and for those coordinates in *Ia*3 where $z$ is in the $a_3$-axial position, a nearest group whose elements are in both is *Ibca*. The orthorhombic group contains half the elements in $I4_1/acd$ and one-third the elements in *Ia*3. Since its equivalent point set has sixteen elements, it remains to inquire if the three non-equivalent oxygens for braunite match with three coordinates for the oxygens in bixbyite. Indeed, these can be found, and they are O(1) = (0.149, −0.146, −0.110) (0.129, −0.147, −0.084); O(2) = (0.146, 0.073, 0.114), (0.147, 0.084, 0.128); and O(3) = (0.079, 0.135, −0.150), (0.083, 0.129, −0.146) for braunite and bixbyite respectively. Since the bixbyite cell shape was chosen, the $z$ coordinates in braunite were doubled. Finally, the coordinate for oxygen reported

[1] To receive a copy of this material, order document AM-76-031 from the Business Office, Mineralogical Society of America, 1909 K Street, N.W., Washington, D.C. 20006. Please remit $1.00 in advance for the microfiche.

TABLE 3. Braunite. Anisotropic thermal vibration parameters ($\times 10^4$)*

| | $\beta_{11}$ | $\beta_{22}$ | $\beta_{33}$ | $\beta_{12}$ | $\beta_{13}$ | $\beta_{23}$ |
|---|---|---|---|---|---|---|
| Mn(1) | 35.0(27) | = $\beta_{11}$ | 4.3(4) | -24.1(15) | 0 | 0 |
| Mn(2) | 14.9(8) | 17.6(9) | 3.8(2) | - 3.3(7) | -1.4(4) | 0.3(3) |
| Mn(3) | 17.0(9) | 13.7(9) | 4.1(2) | 0 | 1.2(4) | 0 |
| Mn(4) | 15.5(12) | = $\beta_{11}$ | 3.8(2) | - 1.7(6) | -0.2(5) | = $-\beta_{23}$ |
| Si | 13.0(24) | = $\beta_{11}$ | 4.8(6) | 0 | 0 | 0 |
| O(1) | 23.8(31) | 18.8(30) | 5.5(8) | 1.7(23) | -0.5(13) | -0.2(13) |
| O(2) | 15.5(30) | 14.6(30) | 5.8(8) | - 2.3(21) | -0.8(13) | 3.1(12) |
| O(3) | 22.6(32) | 15.5(31) | 6.7(8) | 0.7(23) | -2.3(13) | 0.6(12) |

*Coefficients in $\exp[-(\beta_{11}h^2 + \beta_{22}k^2 + \beta_{33}\ell^2 + 2\beta_{12}hk + 2\beta_{13}h\ell + 2\beta_{23}k\ell)]$.

by Geller (1971) was reoriented to conform with the transformation *Pcab* → *Pbca*.

Inspection of the space group *Ibca* (Table 7) reveals that eight symmetry elements are generated by the composition of symmetry elements $[1,i(1)]\cdot[1,a_{(b)},b_{(a)},2_{(c)}]$ and the remaining eight by the composition of these with $[1,2_{1(c)}]$. For the real bixbyite and braunite crystals, $[1,a_{(b)},b_{(a)},2_{(c)}]$ generate a sheet of crystal structure which is isomorphic in both crystals. The composition with $i(1)$ leads to completed octahedral sheets, and these with $[1,2_{1(c)}]$ leads to equivalent sheets which are translated $(1/2+z)$ in bixbyite. In braunite, the composition with $4_{1(c)}$ in place of $2_{1(c)}$ leads to equivalent sheets displaced $(1/4+z)$, $(1/2+z)$, and $(3/4+z)$. Therefore, we conclude that bixbyite and braunite contain sheets which are locally isomorphic to each other and which occur at $(z+m/2)$ in bixbyite and $(z+m/4)$ in braunite, where $m$ is an integer. Call these the *A* sheets. The distinct kind of sheets at $[z'+(2m+1)/8]$ in braunite we call the *B* sheets.

Light is cast on the interesting phase, braunite-II, first described by de Villiers and Herbstein (1967). For this phase, the *c* axis of braunite is doubled (Table 1), but the space group remains unchanged. The ideal formula is $Mn_{15}SiO_{24}$ or $Mn^{2+}Mn^{3+}_{14}SiO_{24}$. We now propose a structure for this phase. Consider bixbyite in *Pbca* orientation. Since *Pbca* is a sub-

TABLE 4. Braunite. Parameters for the ellipsoids of vibration*

| Atom | i | μi | θia | θib | θic | B(Å$^2$) | Atom | i | μi | θia | θib | θic | B(Å$^2$) |
|---|---|---|---|---|---|---|---|---|---|---|---|---|---|
| Mn(1) | 1 | 0.070(8) | 45 | 45 | 90 | 1.03(7) | Si | 1 | 0.076(7) | - | - | - | 0.53(6) |
| | 2 | 0.087(5) | 90 | 90 | 180 | | | 2 | 0.076(7) | - | - | - | |
| | 3 | 0.163(5) | 45 | 135 | 90 | | | 3 | 0.092(6) | 90 | 90 | 0 | |
| Mn(2) | 1 | 0.072(3) | 39 | 69 | 58 | 0.56(2) | O(1) | 1 | 0.090(7) | 73 | 163 | 90 | 0.76(5) |
| | 2 | 0.083(3) | 76 | 53 | 140 | | | 2 | 0.098(7) | 109 | 96 | 160 | |
| | 3 | 0.096(2) | 126 | 45 | 68 | | | 3 | 0.105(7) | 154 | 106 | 70 | |
| Mn(3) | 1 | 0.078(3) | 90 | 0 | 90 | 0.55(2) | O(2) | 1 | 0.070(9) | 108 | 150 | 66 | 0.63(5) |
| | 2 | 0.079(3) | 51 | 90 | 141 | | | 2 | 0.083(8) | 158 | 80 | 109 | |
| | 3 | 0.092(2) | 39 | 90 | 51 | | | 3 | 0.109(7) | 102 | 62 | 31 | |
| Mn(4) | 1 | 0.079(4) | 45 | 45 | 90 | 0.54(3) | O(3) | 1 | 0.082(8) | 78 | 164 | 79 | 0.76(5) |
| | 2 | 0.081(3) | 98 | 82 | 169 | | | 2 | 0.094(7) | 145 | 105 | 121 | |
| | 3 | 0.088(3) | 134 | 46 | 79 | | | 3 | 0.115(6) | 123 | 87 | 33 | |

*i = ith principal axis; $\mu_i$ = rms amplitude; $\theta_{ia}$, $\theta_{ib}$, $\theta_{ic}$ = angles between the ith principal axis and the cell axes $\underline{a}_1$, $\underline{a}_2$ and $\underline{c}$. The equivalent isotropic thermal vibration parameters are also stated.

TABLE 6. Braunite. Polyhedral interatomic distances and angles*

| | | |
|---|---|---|
| **Mn(1)** | | |
| 4 Mn(1)-O(1)$^{(1)}$ | 2.153(5)Å | |
| 4 -O(2) | 2.501(6) | |
| average | 2.327 | |
| 2 O(2) -O(2)$^{(8)}$ | 2.576(6) | 62.0(1) |
| 4 O(2) -O(1)$^{(3)}$ | 2.638(6) | 68.6(1) |
| 2 O(1)$^{(3)}$-O(1)$^{(6)}$ | 2.694(8) | 77.5(2) |
| 4 O(2) -O(1)$^{(1)}$ | 2.853(7) | 75.2(1) |
| average | 2.709 | 71.2 |
| 2 O(1)$^{(1)}$-O(1)$^{(6)}$ | | 164.0(2) |
| 2 O(2) -O(2)$^{(9)}$ | | 170.6(2) |
| **Si** | | |
| 4 Si -O(3)$^{(2)}$ | 1.612(4) | |
| 2 O(3)$^{(2)}$-O(3)$^{(5)}$ | 2.626(8) | 109.1(2) |
| 4 O(3)$^{(2)}$-O(3)$^{(6)}$ | 2.635(7) | 109.6(1) |
| average | 2.632 | 109.3 |
| **Mn(2)** | | |
| Mn(2)-O(2) | 1.866(2) | |
| -O(2)$^{(1)}$ | 1.866(2) | |
| -O(3) | 2.028(5) | |
| -O(3)$^{(1)}$ | 2.028(5) | |
| -O(1) | 2.212(5) | |
| -O(1)$^{(1)}$ | 2.212(5) | |
| average | 2.035 | |
| O(2) -O(3) | 2.605(6) | 83.9(2) |
| O(2)$^{(1)}$-O(3)$^{(1)}$ | 2.605(6) | 83.9(2) |
| O(1) -O(3) | 2.751(7) | 80.8(1) |
| O(1)$^{(1)}$-O(3)$^{(1)}$ | 2.751(7) | 80.8(1) |
| O(2) -O(1)$^{(1)}$ | 2.854(7) | 88.4(2) |
| O(2)$^{(1)}$-O(1) | 2.854(7) | 88.4(2) |
| O(2) -O(3)$^{(1)}$ | 2.898(7) | 96.1(2) |
| O(2)$^{(1)}$-O(3) | 2.898(7) | 96.1(2) |
| O(2) -O(1) | 2.934(7) | 91.6(2) |
| O(2)$^{(1)}$-O(1)$^{(1)}$ | 2.934(7) | 91.6(2) |
| O(3) -O(1)$^{(1)}$ | 3.232(8) | 99.2(1) |
| O(3)$^{(1)}$-O(1) | 3.232(8) | 99.2(1) |
| average | 2.879 | 90.0 |
| O(1) -O(1)$^{(1)}$ | | 180.0(0) |
| O(2) -O(2)$^{(1)}$ | | 180.0(0) |
| O(3) -O(3)$^{(1)}$ | | 180.0(0) |
| **Mn(3)** | | |
| 2 Mn(3)-O(1)$^{(3)}$ | 1.906(5) | |
| 2 -O(2) | 1.971(6) | |
| 2 -O(3) | 2.267(5) | |
| average | 2.048 | |
| 2 O(2) -O(3) | 2.605(6) | 75.5(2) |
| 2 O(2) -O(1)$^{(3)}$ | 2.638(6) | 85.7(2) |
| 2 O(2) -O(3)$^{(2)}$ | 2.678(6) | 78.0(2) |
| 1 O(1)$^{(3)}$-O(1)$^{(4)}$ | 2.792(8) | 94.2(2) |
| 1 O(2) -O(2)$^{(2)}$ | 2.892(1) | 94.4(3) |
| 2 O(3) -O(1)$^{(3)}$ | 3.246(8) | 101.8(1) |
| 2 O(1)$^{(4)}$-O(3) | 3.312(8) | 104.7(1) |
| average | 2.887 | 90.0 |
| 1 O(3) -O(3)$^{(2)}$ | | 140.7(2) |
| 2 O(2) -O(1)$^{(4)}$ | | 179.8(1) |
| **Mn(4)** | | |
| Mn(4) -O(1)$^{(6)}$ | 1.946(5) | |
| -O(2)$^{(4)}$ | 1.921(3) | |
| -O(1)$^{(3)}$ | 1.946(5) | |
| -O(2)$^{(10)}$ | 1.921(3) | |
| -O(3)$^{(3)}$ | 2.240(5) | |
| -O(3)$^{(6)}$ | 2.240(5) | |
| average | 2.036 | |
| O(1)$^{(6)}$ -O(1)$^{(3)}$ | 2.694(8) | 87.6(2) |
| O(2)$^{(4)}$ -O(2)$^{(10)}$ | 2.576(6) | 84.2(3) |
| O(3)$^{(3)}$ -O(1)$^{(3)}$ | 2.751(7) | 81.8(1) |
| O(3)$^{(6)}$ -O(2)$^{(10)}$ | 2.678(6) | 79.7(2) |
| O(1)$^{(6)}$ -O(3)$^{(6)}$ | 2.751(7) | 81.8(1) |
| O(2)$^{(4)}$ -O(3)$^{(3)}$ | 2.678(6) | 79.7(2) |
| O(1)$^{(6)}$ -O(2)$^{(10)}$ | 2.831(7) | 94.1(2) |
| O(2)$^{(4)}$ -O(1)$^{(3)}$ | 2.831(7) | 94.1(2) |
| O(1)$^{(6)}$ -O(3)$^{(3)}$ | 3.168(8) | 98.1(1) |
| O(2)$^{(4)}$ -O(3)$^{(6)}$ | 3.201(8) | 100.3(2) |
| O(1)$^{(3)}$ -O(3)$^{(6)}$ | 3.168(8) | 98.1(1) |
| O(2)$^{(10)}$-O(3)$^{(3)}$ | 3.201(8) | 100.3(2) |
| average | 2.877 | 90.0 |
| O(3)$^{(3)}$ -O(3)$^{(6)}$ | | 179.9(2) |
| O(1)$^{(6)}$ -O(2)$^{(4)}$ | | 177.0(1) |
| O(1)$^{(3)}$ -O(2)$^{(10)}$ | | 177.0(1) |

*Similar regions of Mn(2) and Mn(4) are listed for comparison, explained in the text. Based on the list in Table 2, the equivalent points are (1) -x, -y, -z; (2) 1/2-x, y, -z; (3) x, 1/2+y, -z; (4) 1/2-x, 1/2+y, z; (5) 1/2+x, 1/2-y, -z; (6) 1/4+y, 1/4+x, 1/4+z; (7) -x, 1/2-y, z; (8) 1/4-y, 1/4-x, 1/4-z; (9) 3/4+y, 1/4+x, 1/4-z; (10) 1/4+y, 3/4-x, 1/4-z; (11) 1/2-x, 1/2-y, 1/2-z; (12) -x, y, 1/2+z; (13) x, -y, 1/2-z; (14) 3/4-y, 1/4-x, 1/4+z.

group of *Ibca* and conserves $2_{1(c)}$, it follows that there are two kinds of sheets normal to the $c$ axis. Call these the $A$ and $A'$ sheets respectively. For cubic bixbyite, these sheets would be equivalent. The cell repeat for orthorhombic bixbyite is $\cdots [AA']_2 \cdots$ with the $z$ translation being $(z_A+2m/4)$ for $A$; and $[z_{A'}+(2m+1)/4]$ for $A'$. For braunite, the cell repeat is $\cdots [AB]_4 \cdots$ with the $z$ translation being

TABLE 7. Group multiplication table for the symmetry elements in *Ibca**

| | \| | I | i(1) | i(2) | $2_1$(c) | $2_1$(b) | $2_1$(a) | 2(c) | 2(b) | 2(a) | c(b) | b(a) | a(c) | c(a) | b(c) | a(b) |
|---|---|---|---|---|---|---|---|---|---|---|---|---|---|---|---|---|
| \| | \| | I | i(1) | i(2) | $2_1$(c) | $2_1$(b) | $2_1$(a) | 2 (c) | 2 (b) | 2 (a) | c (b) | b (a) | a (c) | c (a) | b (c) | a (b) |
| I | | \| | i(2) | i(1) | 2 (c) | 2 (b) | 2 (a) | $2_1$(c) | $2_1$(b) | $2_1$(a) | a (b) | c (a) | b (c) | b (a) | a (c) | c (b) |
| i(1) | | | \| | I | a (c) | c (b) | b (a) | b (c) | a (b) | c (a) | $2_1$(b) | $2_1$(a) | $2_1$(c) | 2 (a) | 2 (c) | 2 (b) |
| i(2) | | | | \| | b (c) | a (b) | c (a) | a (c) | c (b) | b (a) | 2 (b) | 2 (a) | 2 (c) | $2_1$(a) | $2_1$(c) | $2_1$(b) |
| $2_1$(c) | | | | | \| | $2_1$(a) | $2_1$(b) | I | 2 (a) | 2 (b) | b (a) | c (b) | i (i) | a (b) | i (2) | c (a) |
| $2_1$(b) | | | | | | \| | $2_1$(c) | 2 (a) | I | 2 (c) | i (1) | a (c) | b (a) | b (c) | c (a) | i (2) |
| $2_1$(a) | | | | | | | \| | 2 (b) | 2 (c) | I | a (c) | i (1) | c (b) | i (2) | a (b) | b (c) |
| 2(c) | | | | | | | | \| | $2_1$(a) | $2_1$(b) | c (a) | a (b) | i (2) | c (b) | i (1) | b (a) |
| 2(b) | | | | | | | | | \| | $2_1$(c) | i (2) | b (c) | c (a) | a (c) | b (a) | i (1) |
| 2(a) | | | | | | | | | | \| | b (c) | i (2) | a (b) | i (1) | c (b) | a (c) |
| c(b) | | | | | | | | | | | \| | $2_1$(c) | $2_1$(a) | 2 (c) | 2 (a) | I |
| b(a) | | | | | | | | | | | | \| | $2_1$(b) | I | 2 (b) | 2 (c) |
| a(c) | | | | | | | | | | | | | \| | 2 (b) | I | 2 (a) |
| c(a) | | | | | | | | | | | | | | \| | $2_1$(b) | $2_1$(c) |
| b(c) | | | | | | | | | | | | | | | \| | $2_1$(a) |
| a(b) | | | | | | | | | | | | | | | | \| |

*The elements mean the following: | is the identity, I the body-centering; i(1) the inversion at the origin, i(2) the inversion at $(\frac{1}{4}\ \frac{1}{4}\ \frac{1}{4})$. For screws and rotations, the axes to which they are parallel are in parentheses. For glide planes, the parentheses refer to the axes to which these planes are normal.

$(z_A+2m/8)$ for $A$, and $[z_B+(2m+1)/8]$ for $B$. For braunite-II, the postulated sequence is $\cdots[A'BA]_4\cdots$ with the $z$ translation being $\cdots[z_A+(4m+1)/16]$ and $[z_A+(4m+3/16)]$ for A; $(z_{A'}+4m/16)$ for $A'$; and $[z_B+(4m+2)/16]$ for $B$. We note that each $B$ is adjacent to two $A$'s in the braunites. In order to conserve the symmetry elements of the $B$ slab, an $A$ slab is placed at the origin for bixbyite and braunite; and the $A'$ slab is at the origin for braunite-II. The next sequence would be $\cdots[AA'AA'AB]_4\cdots$ with the $A$ slab at the origin and the $z$ translation of $B$ being $[z_B+(6m+3)/24]$. Such long sequences are probably unstable for they require a long-range order between the $B$ layers. Very long sequences, of course, are expressions of an epitaxial relationship between blocks of bixbyite and braunite structures.

If our interpretation of braunite-II proves to be correct, it would appear that the presence of a $B$ slab requires a quadrupling of the sequence in brackets to achieve the $c$-axial repeat, and that each $B$ is bounded on either side by $A$. All such sequences would possess space group $I4_1/acd$.

Mention should be made about the difference between the structure of braunite proposed by Byström and Mason (1943) and our structure. First, we note that $S(I4_1/acd)\cap S(I\bar{4}c2) = S(I\bar{4}c2)$, so the space group selected by Byström and Mason is contained in the holosymmetric group and the application of $4_1$ in place of $2_1$ in $I\bar{4}c2$ generates $I4_1/acd$. Furthermore, if the origin of their cell is shifted by $(0, -1/4, 1/8)$, near-coincidence of their atomic cordinate parameters can be found with ours (Table 8). The *only* exception is their O(1) $x$-parameter [linked to their Si(1)], which has a reversed sense of direction. Two noteworthy results obtain from this difference: first, the reversed direction of O(1) destroys the $4_1$-screw axis in $I4_1/acd$, and second, the $Mn^{3+}$ cations in the A sheet remain in octahedral coordination but with changed orientation. These observations emphasize the strong homometric character inherent in the braunite structure. We suspect that with their limited data set, Byström and Mason could not have resolved the ambiguity in the choice of orientation for the $Si(1)O(1)_4$ tetrahedron. Excluding the ambiguity in O(1), their structure agrees with ours in every detail, and their analysis is praiseworthy in light of the unusual difficulty inherent in the analysis of the structure of braunite.

## Description of the structure

Braunite is based on the packing of cubes [Mn(1)]; octahedra [Mn(2), Mn(3), and Mn(4)]; and tetrahedra (Si). Excepting the $SiO_4$ tetrahedron, the polyhedra are substantially distorted away from regular geometry, and these will be discussed in detail in the next section.

The most convenient description is based on the $A$ and $B$ sheets. The $A$ sheets, oriented parallel to {001}

TABLE 8. Comparison of atomic coordinate parameters for braunite*

| Byström and Mason (1943)* | | | | This Study | | | |
|---|---|---|---|---|---|---|---|
| Mn(1) | 0 | 1/4 | 1/8 | Mn(1) | 0 | 1/4 | 1/8 |
| Mn(2) | 0 | 3/4 | 7/8 | $Mn(1)^{(1)}$ | 0 | 3/4 | 7/8 |
| Mn(3) | 0.236 | 3/4+x | 7/8 | $Mn(4)^{(3)}$ | 0.232 | 3/4+x | 7/8 |
| Mn(4) | .236 | 1/4+x | 1/8 | Mn(4) | .232 | 1/4+x | 1/8 |
| Mn(5) | .264 | .236 | .000 | Mn(3) | 1/4 | .216 | 0 |
| Mn(6) | .264 | .236 | .250 | $Mn(2)^{(6)}$ | 1/4 | 1/4 | 1/4 |
| Si(1) | 0 | 1/4 | 7/8 | $Si^{(12)}$ | 0 | 1/4 | 7/8 |
| Si(2) | 0 | 3/4 | 1/8 | $Si^{(13)}$ | 0 | 3/4 | 1/8 |
| O(1) | .104 | .340 | .927 | $O(3)^{(7)}$ | - .079 | .365 | .925 |
| O(2) | .129 | .619 | .942 | $O(2)^{(3)}$ | .146 | .573 | .943 |
| O(3) | .132 | .386 | .058 | $O(1)^{(3)}$ | .149 | .354 | .055 |
| O(4) | .104 | .659 | .073 | $O(3)^{(3)}$ | .079 | .635 | .075 |
| O(5) | .135 | .884 | .942 | O(1) | .149 | .854 | .945 |
| O(6) | .132 | .112 | .058 | O(2) | .146 | .073 | .057 |
| space group | $I\bar{4}c2$ | | | | $I4_1/acd$ | | |

*After shifting origin (0 -1/4 1/8). The equivalent positions, listed as superscripts, are provided in Table 6.

and situated at $z$ = 0, 1/4, 1/2, and 3/4, are isomorphic to the $A$ and $A'$ sheets in bixbyite. Figures 1a and 1b afford a comparison between the $A$ sheets in braunite and bixbyite. In braunite, the Mn(2) and Mn(3) atoms define a planar checkerboard, and their octahedra form a sheet through corner- and edge-sharing. If the octahedra were regular, a sheet of cubic close-packing would appear, since along one direction, edges would be shared, and orthogonal to it, corners would be shared. Along a row in the

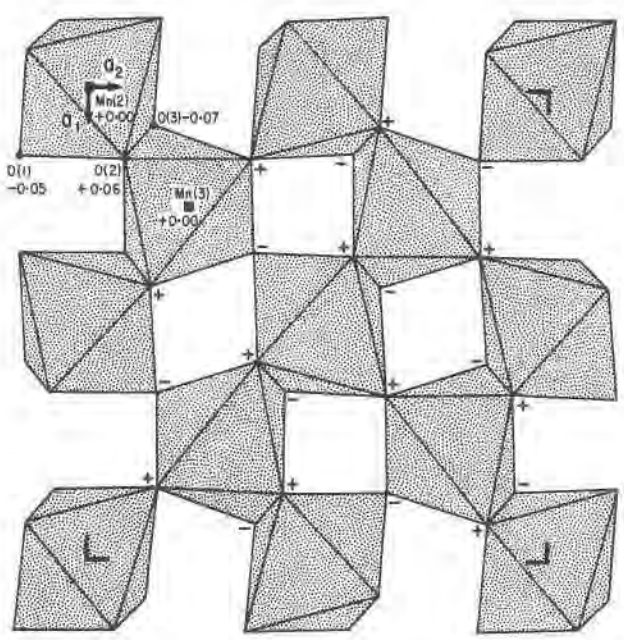


FIG. 1A The $A$ sheet in the braunite crystal structure. Locations of nonequivalent atoms conform to Table 2.

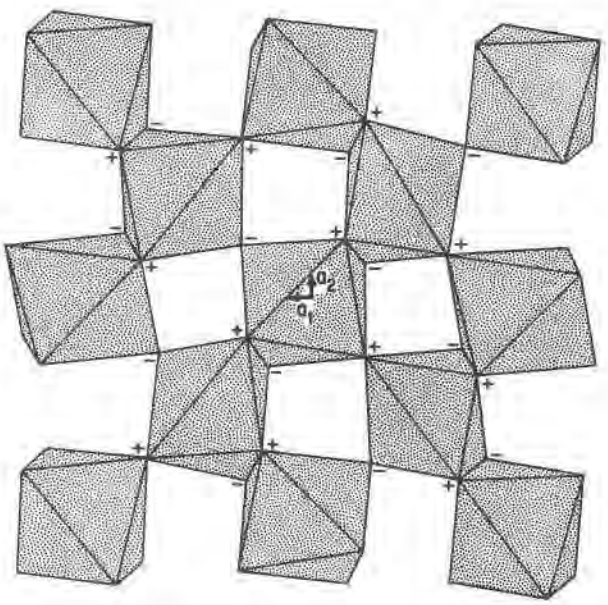


FIG. 1B. The $A$ sheet in the bixbyite crystal structure drawn from the coordinates of Geller (1971). The origin of the cell in that study is shown, the sheet reoriented for convenient comparison with Fig. 1a.

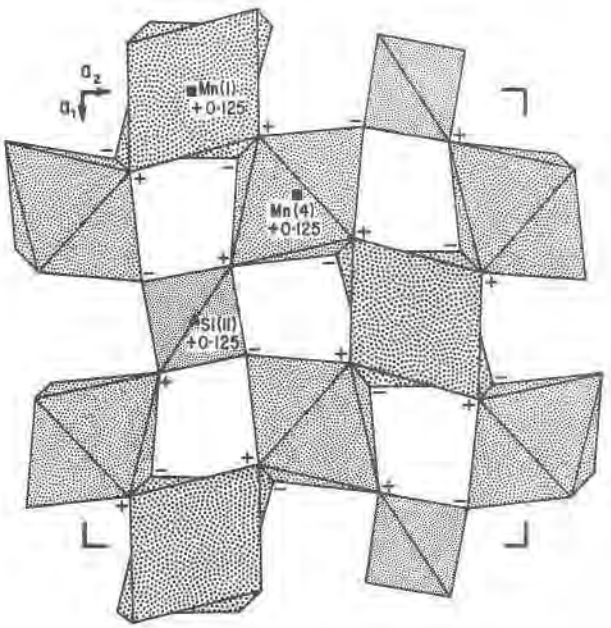


FIG. 2A The *B* sheet in braunite Note tetrahedral, octahedral, and cubic coordination for Si, Mn(4), and Mn(1) respectively.

braunite and bixbyite *A*-sheets, the edge-sharing occurs in units of three octahedra and is then interrupted by corner-sharing; this arises from a major departure of the $Mn(3)O_6$ octahedron away from the $2/m$ symmetry implicit in the cubic dense-packed sheet.

The *B* layer (Fig. 2a) is not isomorphic to the *A'* (= *A*) layer in bixbyite (Fig. 2b). These sheets, also oriented parallel to {001}, are situated at $z$ = 1/8, 3/8, 5/8, and 7/8 in braunite, and consist of linked $Mn(1)O_8$ cubes, $Mn(4)O_6$ distorted octahedra, and $SiO_4$ tetrahedra. Although the cations define a checkerboard pattern and although the oxygens between the A- and B-layer cations are isomorphic to those in bixbyite, only eight of the twelve oxygens above the plane of the B-layer cations are isomorphic in the two structures. Fig. 2b shows that four oxygens [two O(7) oxygens and two O(10) oxygens of Geller (1971)] must be "shuffled" to achieve isomorphism of the bixbyite *A*-layer with the braunite *B*-layer. The group–subgroup relations require that *some* equivalent points in $Ia3$ are not isomorphic to points in $I4_1/acd$. Based on the braunite cell, these include the $4\times2\times2 = 16$ atoms requiring shuffling. In Figure 2b, it is seen that from shuffling the *C* polyhedron receives two additional coordinating oxygens to form a distorted cube, and the *D* polyhedron loses two to form a distorted tetrahedron. Finally, polyhedron *E* achieves a more regular octahedral coordination.

The "shuffling" of anions disguises a deeper relation of the braunite and bixbyite structures. Braunite, bixbyite, pyrochlore, and several more complex structure types are derivative structures of the fluorite structure type and are obtained from an ordered deficit of anions. Figure 3a features the regular fluorite checkerboard as a system of edge-linked cubes. One route of ordering anion vacancies (□) leads to the important pyrochlore $X_2^{(8)}M_2^{(6)}O_7\square$ structure type (Fig. 3b). How many discrete ordered holes are there on the vertices of the cube? Utilizing Pólya's (1937) enumeration theorem, there are twenty-three discrete arrangements, discussed in Appendix I and shown in Figure 6. It is immediately seen that fluorite is based on the $u^8(1)$ arrangement alone; pyrochlore on $u^8(1)$ and ${}^6d^2(3)$; bixbyite on $u^6d^2(2)$ and $u^6d^2(3)$; and braunite on $u^8(1)$; $u^6d^2(2)$, $u^6d^2(3)$; and $u^4d^4(4)$, that is, the cube, two kinds of distorted octahedra, and the tetrahedron, respectively. Thus, braunite is in one sense a shuffled bixbyite, but in another sense a novel structure type based on a different combination of ordered anion vacancies over the fluorite structure type. Enumeration of ordered holes in lattices derives from Appendix I, and in Appendix II a cooperative lattice game is proposed to characterize these arrangements in a quick and straightforward way.

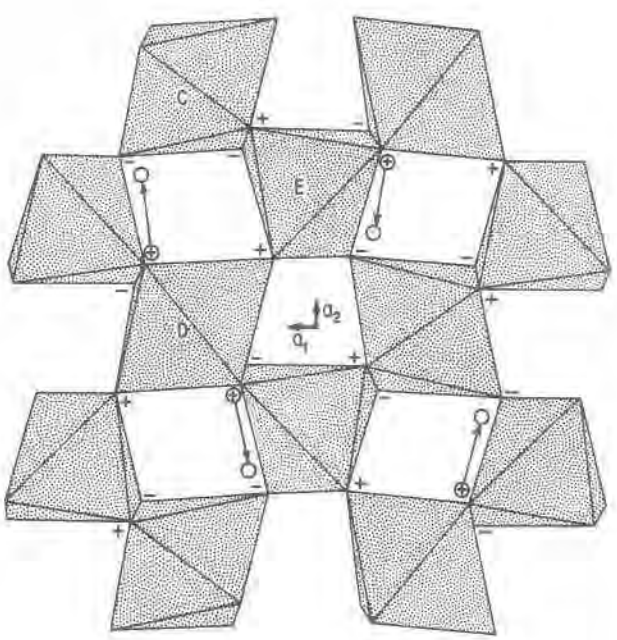


FIG 2B. The *A'* sheet in bixbyite, oriented for direct comparison with Fig 2a. The coordinates are from Geller (1971) The arrows show the atoms which must be shuffled to create the *B* sheet in braunite

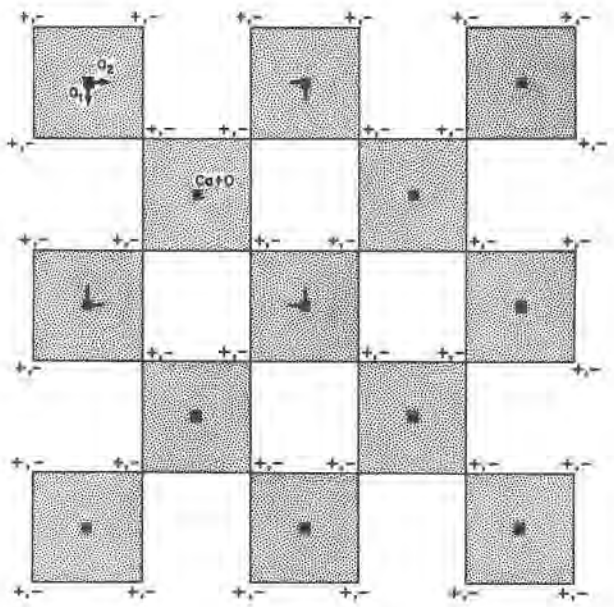


FIG. 3A. The unit checkerboard representing the fluorite arrangement.

### Bond distances, angles and their distortions

A major problem in describing the bond distances, angles, and their distortions for braunite is the combined effect of the severe Jahn-Teller distortion of the $Mn^{3+}O_6$ octahedra, the relation to the fluorite structure type, and the presence of shared polyhedral edges. The bond distances and angles are listed in Table 6; atom designations and the shared edges are conveniently shown as Schlegel diagrams in Figure 4. These diagrams are the planar maps of the three-dimensional polyhedra and conserve order of vertices and paths along edges. The $Mn(2)O_6$ and $Mn(4)O_6$ octahedra are similar in that their six shared edges define Hamiltonian paths which are isomorphic to each other with respect to the elongated $Mn^{3+}$–$O^{2-}$ bonds. The opposing pair of elongated bonds arising from the *d* high-spin electronic distribution in a weak crystal field are called the *apical* bonds, and the four shortened planar bonds are called the *meridional* bonds.

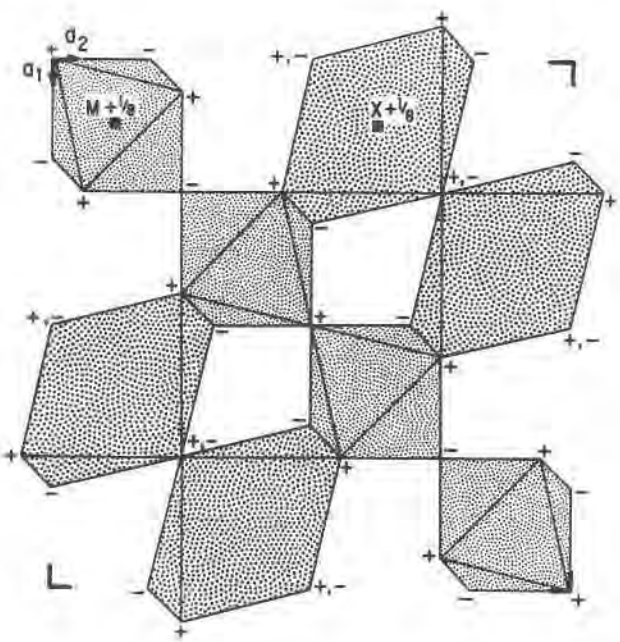


FIG. 3B. The unit sheet representing the crystal structure of pyrochlore. Note octahedral coordination about *M* and cubic coordination about *X*.

The $Mn(2)O_6$ octahedron of point symmetry $\bar{1}$ has a distribution of shared edges and apical bonds which suggests $2/m$ pseudosymmetry, as does the $u^6d^2(3)$ arrangement. Indeed, listing the bond distances and angles in Table 6 according to the "equivalent" distances for $2/m$ shows that deviations range at most about 0.1Å for O–O′ edges and about 3° for O–Mn(2)–O′ angles. The apical bonds are 2Mn(2)–O(1) = 2.21Å and the meridional bonds are 2Mn(2)–O(2) = 1.87Å and 2Mn(2)–O(3) = 2.03Å. We shall demonstrate later that the splitting of the meridional bonds by 0.16Å is a consequence of deviations from local electrostatic neutrality. The Mn(4)–O(6) octahedron of point symmetry 2 likewise possesses $2/m$ pseudosymmetry, but this is more seriously degraded than in $Mn(2)O_6$ by the unsymmetrical distribution of nearest-neighbor edge-sharing polyhedra, the $Mn(1)O_8$ cube distributed such that the $2/m$ pseudosymmetry is broken. As a result, "equivalent" O–O′ distances deviate by as much as 0.3Å and angles by 8°. The apical bonds are 2Mn(4)–O(3) = 2.24Å, and the meridional bonds are 2Mn(4)–O(1) = 1.95Å and 2Mn(4)–O(2) = 1.92Å; owing to local electrostatic neutrality, the meridional bonds are split by only 0.03Å. Bond distances for Mn(2) and Mn(4) are listed in Table 6 as increasing values for Mn(2); those listed for Mn(4) are according to the isomorphism of the Schlegel diagrams in Figure 4. It is apparent that Mn(2) and Mn(4) are similar in their geometry.

The $Mn(3)O_6$ octahedron of point symmetry 2, which also shares six of its edges, differs markedly from Mn(2) and Mn(4). Although the Mn(3)–O bond distances are not unusual [2Mn(3)–O(1) = 1.91, 2Mn(3)–O(2) = 1.97, 2Mn(3)–O(3) = 2.27Å], the polyhedron is severely distorted. This is particularly evident if the $O(3)$–$Mn(3)$–$O(3)^{(2)}$ = 141°

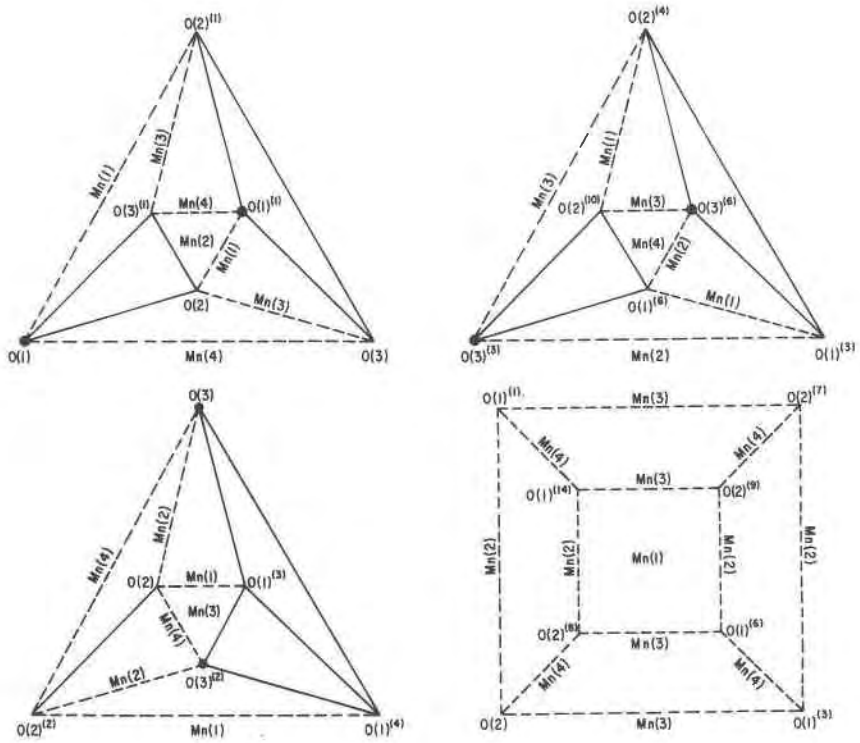


FIG. 4. Schlegel diagrams of the Mn–O polyhedra in braunite. These diagrams show the order of the atom nomenclature as used in Table 6. Shared edges are dashed, and the adjacent cation is listed. The cation in the center of the polyhedron is listed in the center of the diagram. Apical oxygens showing elongate bond distances are drawn as disks.

apical angle is noted, and clearly results from the Mn–Mn repulsions across shared edges. The Schlegel diagram in Figure 4 reveals that the shared edges are along one side of the polyhedron so that Mn(3) moves away from the O(2)–O(2)$^{(2)}$ edge and toward the O(1)$^{(3)}$–O(1)$^{(4)}$ edge. The result is a bending of O(1)–Mn(3)–O(3)$^{(2)}$ by 39° away from regular tetragonal coordination. It is likely that this kind of distortion is a key feature in the stability of braunite and bixbyite structure types, since the polyhedron more closely represents the shape derived from the fluorite cube, which as $u^6d^2(2)$ is a highly distorted octahedron.

The Mn(1)$O_8$ cube of point symmetry 222 shares all twelve of its edges with other polyhedra. It is best described as a twisted cube, and possesses four short 4Mn(1)–O(1)$^{(1)}$ = 2.15Å and four long 4Mn(1)–O(2) = 2.50Å bonds. The average bond distance, Mn(1)–O = 2.33Å, is identical to the value obtained by Shannon and Prewitt (1969) on a garnet structure. The O–Mn(1)–O angles range from 62° to 78° compared with the 70.5° angle for the regular cube. The most significant angular distortions are found for the body diagonals, which deviate from 180° by 9° and 16° as a result of the twist. The $SiO_4$ tetrahedron of point symmetry $\bar{4}$ is nearly regular as only corners are shared with other polyhedra.

## Electrostatic bond strength sums

For spherical ions, the bond strength, $s$, is obtained by dividing the charge of the cation by its coordination number. For minerals and other stable ionic crystals the sum $p_x = \Sigma s_i$ of the $i$ cations bonded to the anion should deviate, $\Delta p_x$, only slightly from the charge of the anion with reversed sign. The deviations correlate with deviations in individual bond distances away from polyhedral averages. Baur (1970) has discussed such calculations and correlations in great detail.

Owing to the non-spherical electron-density distribution about $Mn^{3+}$ (HS), Kampf and Moore (1976) proposed, on empirical grounds, $s = 4/12$ for elongate apical bonds and $s = 7/12$ for the shortened meridional bonds, distinct from $s = 6/12$ for a regular octahedral anion coordination about a spherical trivalent cation. Calculating $\Delta p_x$, we observe that

O(2) has $\Delta p_x = 0.00$, O(1) has $\Delta p_x = -0.25$, and O(3) has $\Delta p_x = +0.25$. The local cation undersaturation about O(1) doubtless correlates with the short Mn(1)–O(1)[1] distances and oversaturated O(3) with the long Mn(2)–O(3) meridional distances observed for braunite.

## Appendix I

*Enumeration of vacancies on the vertices of the cube*

We are interested in the permutation group, $G$, whose elements are based on the point groups $4/m\bar{3}\ 2/m$ (cubic holosymmetric), 432 (cubic enantiomorphic), $4/m\ 2/m\ 2/m$ (tetragonal holosymmetric), and 422 (tetragonal enantiomorphic). The domain, $D$, consists of eight elements, $\{d_1,d_2,\cdots,d_8\}$, which are the eight vertices of the cube or tetragonal prism, and the range, $R$, consists of two elements, $\{u,d\}$. The elements of the range may be conceived as two colors or as statements like "yes" and "no." Here, $d$ corresponds to a vacancy at the vertex of the cube and $u$ to an occupancy. Diagrams of the discrete distributions of vacancies can be conveniently shown as squares (Fig. 6). A vacancy on the vertex above the plane of projection shall be shown as a solid disk, and a vacancy on a vertex below the plane as an open disk.

The cycle indices, $P\{G:D\}$, for the four crystal classes acting upon $D$ are:

$$G\{4/m\bar{3}\ 2/m\} \qquad P\{4/m\bar{3}\ 2/m:D\}$$
$$= \frac{1}{48}\,(x_1^8 + 13x_2^4 + 8x_1^2x_3^2 + 6x_1^4x_2^2 + 8x_2^1x_6^1 + 12x_4^2)$$

$$G\{432\} \qquad P\{432:D\}$$
$$= \frac{1}{24}\,(x_1^8 + 9x_2^4 + 8x_1^2x_3^2 + 6x_4^2)$$

$$G\{4/m\ 2/m\ 2/m\} \quad P\{4/m\ 2/m\ 2/m:D\}$$
$$= \frac{1}{16}\,(x_1^8 + 9x_2^4 + 2x_1^4x_2^2 + 4x_4^2)$$

$$G\{422\} \qquad P\{422:D\} \qquad = \frac{1}{8}\,(x_1^8 + 5x_2^4 + 2x_4^2)$$

The pattern inventories, $F\{P:R\}$, are:

$$P\{4/m\bar{3}\ 2/m:D\} \qquad F\{P:u,d\} =$$
$$u^8 + u^7d + 3u^6d^2 + 3u^5d^3 + 6u^4d^4 + \cdots$$

$$P\{432:D\} \qquad F\{P:u,d\} =$$
$$u^8 + u^7d + 3u^6d^2 + 3u^5d^3 + 7u^4d^4 + \cdots$$

$$P\{4/m\ 2/m\ 2/m:D\}F\{P:u,d\} =$$
$$u^8 + u^7d + 5u^6d^2 + 5u^5d^3 + 10u^4d^4 + \cdots$$

$$P\{422:D\} \qquad F\{P:u,d\} =$$
$$u^8 + u^7d + 6u^6d^2 + 7u^5d^3 + 13u^4d^4 + \cdots$$

Thus, for $G$, $D$, and $R$ as specified, there are 22 discrete arrangements which are distinguishable under cubic holosymmetry, 23 discrete arrangements under the cubic enantiomorphic class, 34 arrangements under the tetragonal holosymmetric, and 43 arrangements under the tetragonal enantiomorphic class. It follows that $|F\{432\}| - |F\{4/m\bar{3}\ 2/m\}| = 1$, the only arrangement having chirality being found in $u^4d^4$. Also, $|F\{422\}| - |F\{4/m\ 2/m\ 2/m\}| = 9$, the chiral arrangments being one in $u^6d^2$, two in $u^5d^3$, three in $u^4d^4$, two in $u^3d^5$, and one in $u^2d^6$.

The configurations are shown diagrammatically in Figure 6. Under each category, $u^rd^s$, those grouped together are equivalent for the cube but distinct for the tetragonal prism. They are coded $u^rd^s(m)$, where $u$ is an occupancy, $r$ the number of occupied sites (= coordination number), $d$, the vacancies of which there are $s$, and $m$ is an integer for codifying. The symbol, "*", means that the arrangement has a chiral mate. Interchanging solid (= above) and open (= below) disks leaves the configuration unchanged, so these are shown by "equal" signs. Thus, $u^4d^4(3)$ is an arrangement on a cube and involves one of the six discrete ways of distributing four vacancies over the cube's vertices. When the tetragonal prism is chosen as the domain, it is broken into two discrete arrangements, $u^4d^4(3)$ and $u^4d^4(3t)$ which are isomorphic over the cubic domain but distinguishable over the tetragonal prismatic domain. Since $S\{4/m\ 2/m\ 2/m\} \subset S\{4/m\bar{3}\ 2/m\}$, the tetragonal prismatic domain has a larger number of discrete configurations.

In Appendix II, these modules shall be used as "players" in a lattice game. Since a tetragonal board is used, there are 34 kinds of players, those acting under the tetragonal holosymmetric class as the basis for the permutation group. Nine of these players have chiral mates. If handedness is counted as distinct, then there are 43 "players." In turn, the 34 kinds of players can be reduced to 22 possible arrangements over the vertices of a cube, with only $u^4d^4(6)$ having a chiral mate. The maximal point symmetries of the arrangements for the two holosymmetric classes as bases for the permutations are given in Table 9.

## Appendix II

*Cooperative lattice games*

The thirty-four discrete patterns in Appendix I can be utilized as "players" in a three-dimensional lattice game. The "board" consists of a checkerboard of any specified planar edge dimensions. The "black" squares of the checkerboard will be called the *unit*

TABLE 9. Point groups for the vacancies at the vertices of a cube*

| | | | | | | | |
|---|---|---|---|---|---|---|---|
| $u^8(1)$ | 4/m $\bar{3}$ 2/m<br>4/m 2/m 2/m | $u^6d^2(3)$ | $\bar{3}$ 2/m<br>2/m | $u^4d^4(1)$ | 4mm<br>4mm | $u^4d^4(4)$ | $\bar{4}$ 3m<br>$\bar{4}$ 2m |
| $u^7d^1(1)$ | 3m<br>m | $u^5d^3(1)$ | m<br>m | $u^4d^4(1t)$ | -<br>2mm | $u^4d^4(5)$ | 3m<br>m |
| $u^6d^2(1)$ | 2mm<br>2mm | $u^5d^3(1t)$ | -<br>1 | $u^4d^4(2)$ | m<br>m | $u^4d^4(6)$ | 2<br>2 |
| $u^6d^2(1t)$ | -<br>m | $u^5d^3(2)$ | m<br>m | $u^4d^4(2t)$ | -<br>1 | $u^4d^4(6t)$ | -<br>1 |
| $u^6d^2(2)$ | 2mm<br>2mm | $u^5d^3(2t)$ | -<br>1 | $u^4d^4(3)$ | 2/m 2/m 2/m<br>2/m 2/m 2/m | | |
| $u^6d^2(2t)$ | -<br>2 | $u^5d^3(3)$ | 3m<br>m | $u^4d^4(3t)$ | -<br>2/m | | |

*After each configuration symbol, the point symmetry of the scheme is given for a cubic domain followed by the symmetry for a tetragonal prismatic domain. Symbols with a "t" in them imply the tetragonal prismatic domain. For $u^sd^r$, where s<r, the symmetry is the same as $u^rd^s$.

*checkerboard*; the "red" squares will be called the *complementary checkerboard.* Four rules are required for play:

*Rule 1.* The unit checkerboard and complementary checkerboard have translational properties, the linear translations corresponding to the vectors of the two edges of the board.

*Rule 2.* Adjacent players can be linked at a common corner only if the symbols of each match. The possible matching symbols at a corner are no disk; solid disk; open disk; or both solid and open disk.

*Rule 3.* The complementary checkerboard adopts open disks in place of solid disks of the unit checkerboard. If open disks or no disks appear on the unit checkerboard no open disk can be placed at that position on the complementary checkerboard. The player is free to add solid disks providing rules 1 and 2 are satisfied.

*Rule 4.* The articulated complementary checkerboard becomes the new unit checkerboard and the game is continued until a repeated pattern along the stacking axis of the boards is achieved.

With respect to the fluorite structure, the unit checkerboard corresponds to a sheet of edge-linked cubes, the players being $u^8(1)$. The complementary checkerboard is also a sheet of edge-linked cubes which share edges with the tops of the cubes of the unit checkerboard below.

Several rather interesting kinds of games can be conceived. Any arrangement of a unit checkerboard which is identical to that of its complementary checkerboard is called *self-complementary.* This means that the same kinds of $u^rd^s(m)$, $u^{r'}$ $d^{s'}$ $(m')\cdots$ occur on both boards and these occur in the same order. The complementary board may have to be rotated to achieve an exact match with the unit checkerboard. This, in effect, admits the existence of screw axes normal to the boards.

The unit checkerboard of pyrochlore (Fig. 5a) is one such example of a self-complementary structure. It is generated from $u^8(1)$ and $u^6d^2(3)$. The board's edges are each twice the length of the fluorite board. The stacking axis requires four boards. A more elegant example of a self-complementary structure is that of calzirtite, $Ca_2ZrZr_4Ti_2O_{16}$ (Fig. 5b). It is generated from $u^8(1)$, $u^7d(1)$, and $u^6d^2(3)$. This structure, too, requires four repeats. The unit board has length three times that of fluorite. All self-complementary structures only require specifications of the unit checkerboard, since the structure is repeated by the appropriate choice and orientation of a screw axis. Thus, in Figures 5a and 5b, the $4_1$-screw axis is added to complete the sequence. Self-replicating patterns are the composition of a two-sided plane group with a screw axis normal to it. We are presently retrieving in a systematic way just those arrangements which are self-complementary.

A curious, and probably rather limited version of

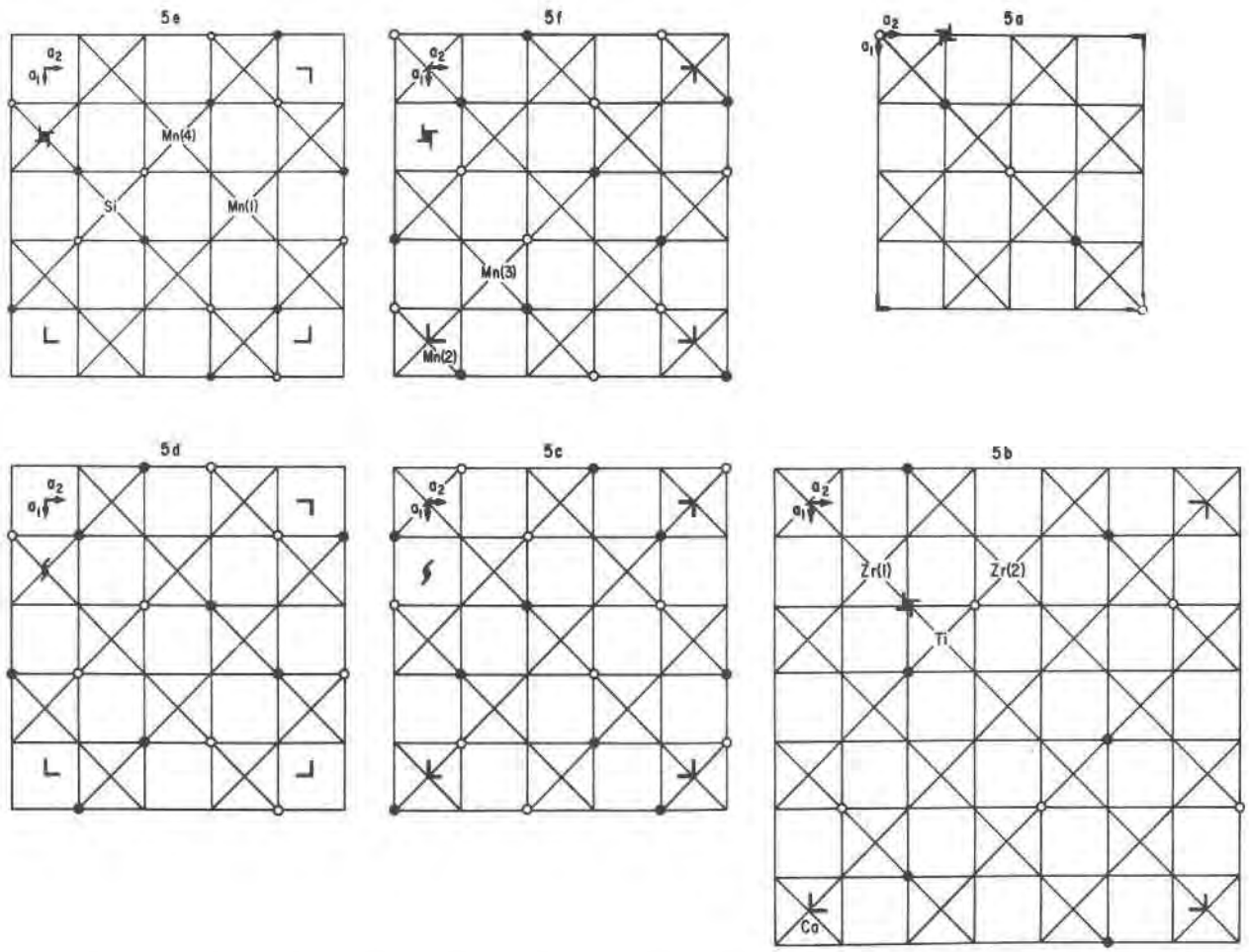


FIG. 5. Checkerboards found in braunite and related structures. Vacancies at the vertices of the cube are shown as solid disks (above) or as open disks (below). The occupied cubes are crossed Loci of screw axes are shown.

(a) Unit board for pyrochlore.
(b) Unit board for calzirtite.
(c) Unit board for bixbyite.
(d) Complementary board for bixbyite.
(e) Complementary board for braunite (compare with 5d).
(f) Unit board for braunite (compare with 5c).

self-complementary arrangements are those we call *pseudo-self-complementary*. In such arrangemented, the kinds of $u^r d^s(m)$, $u^{r'} d^{s'}(m')$, $\cdots$ are the same with respect to $(r,s)$, $(r',s')$, $\cdots$ but the $(m)$, $(m')$, $\cdots$ are *not* all the same. For such arrangements, although the coordination numbers are of the same kind for the articulated boards, the polyhedral shapes are not superimposable. Bixbyite is one such example; in Figure 5c, it is seen that the unit checkerboard consists of $u^6d^2(2t)$ and $u^6d^2(3)$, but the complement (Fig. 5d) consists of $u^6d^2(2)$ and $u^6d^2(2t)$. The structure is repeated by applying the $2_1$-screw to unit and complement. In the actual cubic bixbyite structure, $u^6d^2(2)$ and $u^6d^2(3)$ are distorted so that they are equivalent in the cubic structure. The ease of formation of the orthorhombic structure may reflect the presence of two kinds of vacancy orderings on the undeformed fluorite cubes for the cube, and three kinds for the tetragonal prism. Furthermore, the space group *Pbca* for orthorhombic bixbyite allows the existence of the three kinds of distortions, $u^6d^2(2t)$, $u^6d^2(2)$, and $u^6d^2(3)$.

Structures whose unit and complement do not have the same kinds of $(r,s)$, $(r',s')\cdots$ or in which these are not in the same order are called *non-self-replicating*. For these, freedom in the choice of solid disks on the

complementary board is permissible. The braunite *B*-layer is one such example (Fig. 5e): the pattern, made up of $u^8(1)$, $u^6d^2(3)$, and $u^4d^4(4)$, is not self-replicating since inspection shows that each square on the complementary checkerboard has one open disk. The complement to braunite (Fig. 5f) is recognized as the unit checkerboard of bixbyite. The repeat pattern for braunite is made complete by applying a $4_1$-screw to the composite of unit and complement.

Beyond the mere enjoyment of playing these games, we are extending our study to explore systematically and retrieve all patterns and seek out those structures which satisfy these patterns. We proceed from lines similar to the study of space group genealogies and their application to structure types (see Neubüser and Wondratschek, 1966). Completed three-dimensional composites of boards with the same axial dimensions are called "Zellengleich," and composite boards whose arrangements belong to the same point group are called "Klassengleich." One desirable result is the systematic retrieval of both space group and structure type associated with these patterns. It is clear that the fluorite arrangement is particularly adaptive and admits a range of coordination numbers, from eight to at least three, and we suspect that a large number of as yet unrecognized structure types exist.

Since the checkerboards classify "holes," the task of describing the structures is much easier. In fact, bixbyite, braunite, pyrochlore, and calzirtite are trivial. We are presently exploring structures of rather monstrous size, all of which upon preliminary examination prove to be anion-deficient fluorite derivative structures. These include magnussonite, $32Mn_5(OH)(AsO_3)_3$, $Ia3d$; stenhuggarite, $8Ca_2Fe_2Sb_2O_2(AsO_3)_3$, $I4_1/a$; cafarsite, $4Ca_6Mn_2Fe_4Ti_3(OH)_4(AsO_4)_{12}$, $Pn3$; and, perhaps most complicated of all, parwelite, $16Mn_5SbAsSiO_{12}$, $A2/a$.

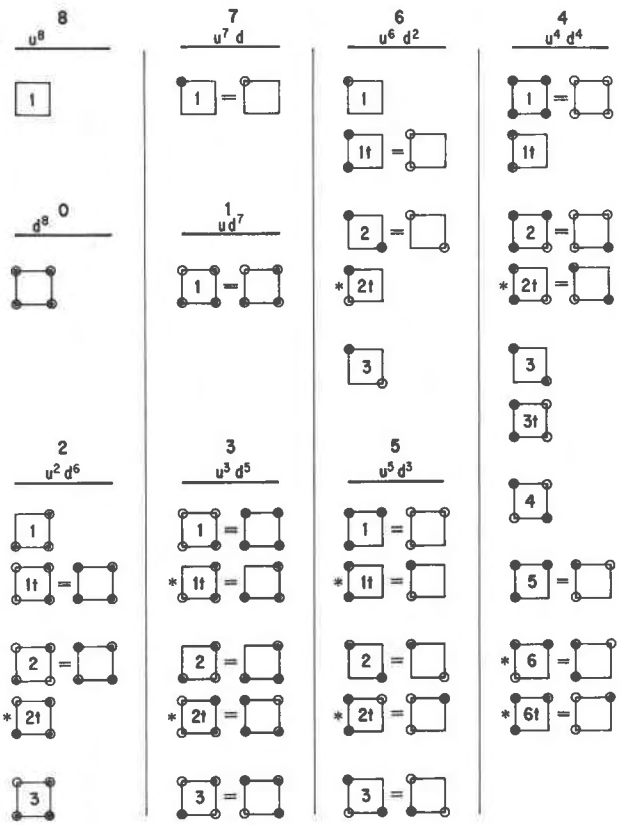


FIG. 6. The discrete vacancies on the vertices of a cube (numerals) and a tetragonal prism (numerals, and numerals plus letters). A vacancy above the plane of projection is shown as a solid disk and a vacancy below the plane as an open disk. Coordination numbers head the patterns. Chiral arrangements are starred. Arrangements which are equivalent by reorientation are shown.

Under $u^4d^4$, for example, there are six kinds of vacancy distributions over the cube (1, 2, 3, 4, 5, and 6) and ten kinds over the tetragonal prism (1, 2, 3, 4, 5, 6, 1*t*, 2*t*, 3*t*, and 6*t*) disregarding chiral mates.

## Addendum

Shortly after this study was submitted for publication, deVilliers (1975) announced solution and refinement of the braunite crystal structure on a sample from Långban, Sweden. The two studies are not only completely independent but proceed from quite different approaches and emphasize quite different aspects of the problem. Therefore, we decided not to alter our manuscript except in response to the suggestions by the referee, which materially improved the text. Readers of both papers will note that de Villiers' study does not mention Jahn-Teller distortion but attributes polyhedral distortion to electrostatic effects, that is, from the local arrangement of nearest-neighbor coordination polyhedra. We believe that this is hardly the complete state of affairs, and our discussion on bond distances and strengths includes *both* the effects of Jahn-Teller distortion *and* electrostatic repulsion across shared edges; Table 6 and the attendant discussion show that consistency is therein obtained. One minor point concerns the stated $M(1)$–O distance of 2.23 Å in the earlier study, which is really 2.34 Å as shown in the table on interatomic distances and should be compared with $Mn^{2+}$ in eight-fold oxygen coordination, not six, from the tables of Shannon and Prewitt (1969).

Regarding the details of the structure refinement, both studies are in good agreement, save for a con-

sistently higher average of about 0.01 Å in bond distances in de Villiers' study, doubtless arising from differences in cell dimensions: $a$ and $c$ are 0.024 Å and 0.035 Å larger than our values. These differences reflect the different techniques in cell refinement, and it is not possible here to ascertain which is closer to the true values. Scientists who tabulate bond distances should be cautioned about this difference in the two studies.

De Villiers emphasizes the importance of silica substitution, which increases to at least 40 weight percent at high temperature. In agreement with de Villiers, we suspect a coupled relationship $Mn^{3+}Mn^{3+} \rightleftarrows Mn^{2+}Si^{4+}$. Indeed, utilizing cooperative lattice games, a large family of derivative structures can be obtained, all consistent with tetragonal cells, but in many instances, suggesting the appearance of superstructure lines.

## Acknowledgments

This study was supported by the National Science Foundation grant NSF GA-40543 (Geochemistry) and through the Materials Research Laboratory grant (NSF) administered to the University of Chicago.

## References

AMINOFF, G. (1931) Lattice dimensions and space group of braunite. *K. Svenska Vetensk. Akad. Handl.* **9,** 14–22.

BAUR, W. H. (1970) Bond length variation and distorted coordination polyhedra in inorganic crystals. *Trans. Am. Crystallogr. Assoc.* **6,** 129–155.

BURNHAM, C. W. (1966) Computation of absorption corrections, and the significance of the end effect. *Am. Mineral.* **51,** 159–167.

BUSING, W. R., K. O. MARTIN and H. A. LEVY (1962) ORFLS, a Fortran crystallographic least-squares program. *U.S. Natl. Tech. Inform. Serv.* ORNL-TM-**305.**

BYSTRÖM, A. AND B. MASON (1943) The crystal structure of braunite, $3Mn_2O_3 \cdot MnSiO_3$. *Ark. Kemi Mineral. Geologi,* **16,** No. 15, 1–8.

CROMER, D. T. AND D. LIBERMAN (1970) *Los Alamos Scientific Laboratory, Univ. of Calif. Rep.* **LA-4403, UC-34.**

——— AND J. B. MANN (1968) X-ray scattering factors computed from numerical Hartree-Fock wave-functions. *Acta Crystallogr.* **A24,** 321–324.

DEVILLIERS,J. P. R. (1975) The crystal structure of braunite with reference to its solid solution behavior. *Am. Mineral.* **60,** 1098–1104.

DE VILLIERS, P. R. AND F. H. HERBSTEIN (1967) Distinction between two members of the braunite group. *Am. Mineral.* **52,** 20–30.

GELLER, S. (1971) Structures of $\alpha$–$Mn_2O_3$, $(Mn_{0.983}Fe_{0.017})_2O_3$ and $(Mn_{0.37}\ Fe_{0.63})_2O_3$ and relation to magnetic ordering. *Acta Crystallogr.* **B27,** 821–828.

GORGEU, A. (1893) Sur les oxydes de manganèse naturels. *Bull. Soc. fr. Mineral.* **16,** 133–148.

HAIDINGER, W. (1831) Mineralogical account of the ores of manganese. *Trans. R. Soc. Edinburgh,* **11,** 119–142.

KAMPF, A. R. AND P. B. MOORE (1976) The crystal structure of bermanite, a hydrated manganese phosphate. *Am. Mineral.* **61,** 000–000.

NEUBÜSER, J. AND H. WONDRATSCHEK (1966) Untergruppen der Raumgruppen. *Kristallogr. Tech.* **1,** 530–543.

PÓLYA, G. (1937) Kombinatorische Anzahlbestimmungen für Gruppen, Graphen, und chemische Verbindungen. *Acta Math.* **68,** 146–254.

RAMACHANDRAN, G. N. AND R. SRINIVASAN (1970) *Fourier Methods in Crystallography.* Wiley-Interscience, New York, p. 96–119.

SHANNON, R. D. AND C. T. PREWITT (1969) Effective ionic radii in oxides and fluorides. *Acta Crystallogr.* **B25,** 925–946.

ZACHARIASEN, W. H. (1968) Experimental tests of the general formula for the integrated intensity of a real crystal. *Acta Crystallogr.* **A24,** 212–214.

*Manuscript received, February 5, 1976;*
*accepted for publication, July 13, 1976.*